© 2013 September 10

Optically induced structural transformation in disordered kesterite Cu₂ZnSnS₄

M. Ya. Valakh[1]), V. M. Dzhagan, I. S. Babichuk, X. Fontane[+], A. Perez-Rodriquez[+*], S. Schorr[×∘]

Lashkaryov Institute of Semiconductor Physics of NAS of Ukraine, 03028 Kyiv, Ukraine

[+]*Catalonia Institute for Energy Research, 08930 Sant Adria del Besos (Barcelona), Spain*

[*]*Departament d'Electronica, Universitat de Barcelona, 08028 Barcelona, Spain*

[×] *Helmholtz-Zentrum Berlin fur Materialien und Energie, D-14109 Berlin, Germany*

[∘]*Freie Universitat Berlin, Institute of Geological Sciences, 12249 Berlin, Germany*

The kesterite-structured semiconductor Cu_2ZnSnS_4 is one of the most promising compound for earth-abundant low-cost solar cells. One of the complex problem on this way deals with its stoichiometry. In this work Raman spectra of Cu-rich Cu_2ZnSnS_4 crystals are discussed in connection with the non-stoichiometric composition and disordering within the cation sublattice of the kesterite. The shift of the main A-peak from 338 to 331 cm^{-1} and its broadening are attributed here to transition from the kesterite ($I\bar{4}$-symmetry) to the disordered kesterite structure ($I\bar{4}2m$-symmetry). It is shown that this transition may also be driven by an intense light, which could stimulate transformation of Cu^+-ion to Cu^{2+}-ions and facilitates generation of Cu_{Zn}-defects on *2d*-crystalographic positions.

Cu_2ZnSnS_4 (CZTS) is a promising material for thin film solar cells due to suitable direct optical gap of about 1.5 eV and large band-to-band optical absorption coefficient (10^5 cm^{-1}) [1–3]. In contrast to better studied CdTe and $Cu_2In(Ga)S(Se)_2$ materials, all constituents of CZTS are non-toxic and abundant in the earth crust. During the last decade the conversion efficiency of CZTS-based solar cells has been improved significantly and values over 11% have been reported recently [4, 5].

However, when moving from binary II–VI to ternary I–III–VI and then to quaternary chalcogenide materials, physico-chemical problems arise related to competing types of crystalline structure, non-stoichiometry, presence of secondary phases of binary and ternary compounds, point defects and their complexes, etc. In the case of CZTS, the latter issues are mainly associated with disordering in the cation sublattice in the form of vacancies (V_{Cu} or V_{Zn}) and anti-sites (Cu_{Zn} or Zn_{Cu}). The possible high concentration of these defects has been observed experimentally [6–8] and discussed theoretically [3, 9–11].

Experimentally, CZTS has been reported to crystallize in the kesterite (KS, $I\bar{4}$-symmetry), the stannite

(ST, $I\bar{4}2m$-symmetry) or the CuAu-like (CA, $P\bar{4}2m$-symmetry) crystal structures. The KS and ST differ only by the ordering of Cu and Zn ions within the cation sublattice. It is generally believed that the ground-state structure of CZTS is KS [3]. However, disorder in the cation sublattice can determine the existence of a third kind of structure for this compound, which has been described as a disordered kesterite structure [9, 12]. The extent of this disorder depends on growth conditions, especially on the deviation from stoichiometry. In the case of Cu-poor (Zn-rich) composition, i.e. when Cu/(Zn+Sn)< 1 the concentration of antisite defects in Cu+Zn crystallographic planes becomes especially large [7]. The situation with random distribution of numerous Cu_{Zn} and Zn_{Cu} defects results in an effective $I\bar{4}2m$-symmetry of the disordered KS structure, which is similar to that of ST [3, 9, 12].

The issue of non-stoichiometry and a presence of native point defects in CZTS is of interest not only from fundamental point of view, but is also important for applications. The matter is that the maximal solar cell efficiency up to now was achieved for a Cu-poor (Zn-rich) structure [4, 5]. However, it is difficult to study the structural problems of CZTS by traditional X-ray diffraction methods only, because of the very similar scattering factors of Cu^+- and Zn^{2+}-ions. Therefore, ad-

[1])e-mail: valakh@isp.kiev.ua

ditional experimental techniques are required. Raman scattering appears to be one of those informative complimentary methods [13–15].

In our recent Raman scattering study of bulk CZTS samples with Cu/(Zn+Sn)$\sim$ 1 [16, 17], we observed an additional peak close to the well known dominant fully-symmetric A-mode of kesterite, located at $338\,\mathrm{cm}^{-1}$. This additional peak (labelled as A* in this report) appears at lower frequency, $332\,\mathrm{cm}^{-1}$, and is characterized by a larger value of the Full Width at Half Maximum (FWHM), compared to the A-mode of the KS (Fig. 1a). The A^*/A intensity ratio depends on the technological conditions under which the samples were prepared. For composition Cu/(Zn+Sn)$\geq$ 1, kesterite structure is favorable [3, 7] and the Raman spectra are dominated by the corresponding A-mode at a frequency of $338\,\mathrm{cm}^{-1}$. The A^*-peak becomes dominant in the Cu-poor (Zn-rich) samples [17] with higher cationic disorder [7]. The latter fact, along with the larger width of the A^* band, allows us to assume the A^* mode to be an indication of the structural disorder of kesterite due to numerous antisite defects [17]. In accordance with [3], the structural disorder is probably accompanied by the change of the symmetry from I$\bar{4}$ to I$\bar{4}$2m. The "defect" origin of the (A^*) mode at $332\,\mathrm{cm}^{-1}$ was also assumed by authors of [18]. Therefore, we can conclude that local deviation from stoichiometry towards Cu/(Zn+Sn) $<$ 1 can stimulate significant disorder in Cu–Zn positions of kesterite crystallographic 2d-sites and can be considered as the "first step" in the structural transformation from the kesterite towards a disordered kesterite structure.

The total lattice energy difference between KS and ST structures is known to be very small, only about $3\,\mathrm{meV/atom}$ [3], due to close Cu and Zn ionic radii. Therefore, based on similarities between these structures and the disordered KS, a similarly small energy difference per atom could be expected between KS and disordered KS structure. Taking this fact into account, we assume that the structural transformation from the KS to a disordered KS can be stimulated by external factors. A possible role of high temperature during the CZTS crystal growth has been discussed previously [17]. Another factor could be an intense laser radiation. It is well known that the process of atomic (ionic) transport in solids can be stimulated by intense optical excitation of the electronic subsystem. The examples are the photoinduced diffusion [19], photo-stimulated transformation of antisite defects in GaAs [20], photoinduced reorientation of structural defects in alkali-halide crystals [21], etc. Searching for possible photoinduced effects in the case of Raman experiments on CZTS crystals, we performed Raman measurements with varied power of
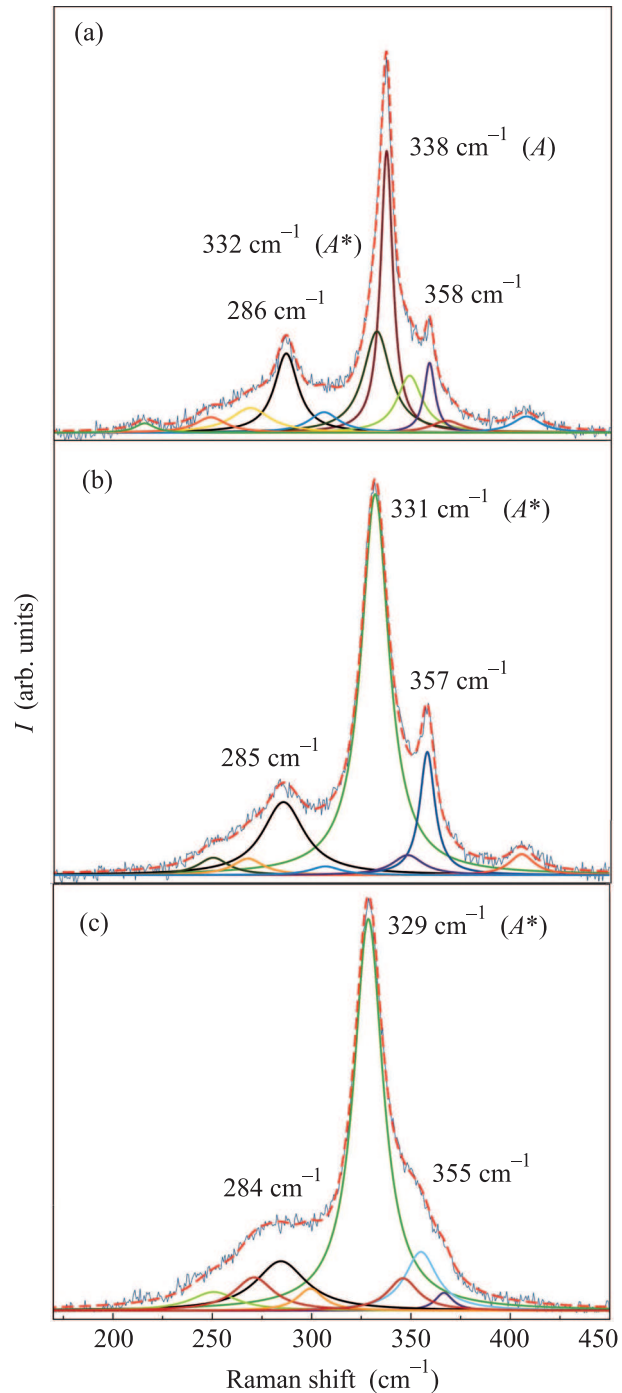
(Color online) Raman spectra of CZTS with the fitting of the peaks with lorentzian curves for the excitation power: $I_0 \sim 0.5\,\mathrm{mW}$ (a), $I = 2I_0$ (b), and $I = 4I_0$ (c) of $\lambda = 514.5\,\mathrm{nm}$

laser excitation. Raman scattering measurements were performed in back scattering configuration with T64000 Horiba Jobin Yvon spectrometer. An Argon–Krypton laser (514.5 nm) was used for excitation, with a 50x objective of an Olympus microscope. Spectra were ob-

tained with different excitation power varied between $\sim 0.5\,\mathrm{mW}$ (I_0) and $2\,\mathrm{mW}$ ($4I_0$). The specimen under study in this work was a single crystal of Cu_2ZnSnS_4, grown by vertical Bridgman method (see reference [17] for details on the samples growth).

Figure show the Raman spectra measured in the same point of the sample surface with different values of the excitation power (I_0, $2I_0$, and $4I_0$), and their fitting with Lorentzian curves. Main contributions in the spectra measured at the lowest excitation power correspond to the A-symmetry kesterite peaks at 286 and $338\,\mathrm{cm}^{-1}$ (the latter labeled in this work as "A-peak") and a peak at $358\,\mathrm{cm}^{-1}$, close to the line at $355\,\mathrm{cm}^{-1}$ that has been reported in [16] as an E/B symmetry peak. The power-dependent changes of the main Raman peak positions and widths are summarized in Table. A complete disappearance of the $338\,\mathrm{cm}^{-1}$ peak and an enhancement of the $332\,\mathrm{cm}^{-1}$ band upon increasing the laser power can be seen on Fig. b. The width of the latter (A^*) band, as compared with Fig. a, is not affected noticeably by increasing the laser power. For the other peaks slight downward shift and broadening are observed. Both broadening and downward shift can be attributed to a heating of the sample by the laser beam, which, according to our estimates, is within several tens of degrees.

Upon further increase of the laser power (Fig. c), the A^*-peak shifts down to $328.5\,\mathrm{cm}^{-1}$. This is due to heating the sample up to $220\pm 20\,^{\circ}\mathrm{C}$. This temperature was estimated from the Stokes/Antistokes intensity ratio measured at this excitation power. The relatively small increase of the FWHM of the A^*-peak is consistent with its disorder-induced origin, with the width of the A^*-peak being mainly determined by inhomogeneous broadening.

Summary of the values of Peak position and FWHM from Figure

Intensity of excitation	Peak Position, cm^{-1}	FWHM, cm^{-1}
	286.4	14.4
	332	16.4
I_0	337.9	6.7
	358	6.6
	285.4	24.8
$2I_0$	331.4	17.0
	357	9.2
	284	31.0
$4I_0$	328.6	17.8
	355	17

In order to distinguish between the purely thermostimulated and photo-stimulated effects in the spectra

obtained at increasing laser power, Raman scattering measurements have also been made in the same region of the samples at the lowest excitation power but heating the sample up to $220\,^{\circ}\mathrm{C}$ with using the Linkam THM600 temperature-controlled stage. The thermal heating of the samples up to this temperature does not lead to noticeable change in the intensity ratio of A and A^*-peaks. The only effect of the pure thermal heating is a downward shift by $3\,\mathrm{cm}^{-1}$ and a noticeable broadening of the kesterite peaks. This demonstrates that changes of spectra in Fig. b and c are not related to the heating of the samples, but are mainly due to an optically-induced increase of antisite defect concentration in CZTS leading to the structural transformation from the KS to the disordered KS structure.

One of the possible mechanisms of the photo-induced increase of the antisite defect concentration in CZTS could be understood via a comparison of the ionic radii of Cu and Zn. Indeed, under excess of Cu^+-ions, interstitial Cu and Zn^{2-} vacancies are expected to be generated. Creation of the antisite defects of Cu^+_{Zn}-type is, however, much less probable because of the significant difference between ionic radius of Cu^+ (95 pm) and Zn^{2+} (74 pm). The situation can change under intense laser illumination, if the latter is capable of ionizing Cu^+- to Cu^{2+}-state. This later state is known to be more favorable [22]. As a result, the formation of Cu^{2+}_{Zn} defects becomes more probable due to the close proximity of the ion radius of Cu^{2+} (72 pm) to that of Zn^{2+} (74 pm). Moreover, the exchange of sites between the latter two isoelectronic ions does not lead to any issues with the charge compensation. The presence of Cu^{2+}-defects in CZTS is a known experimental fact, as shown by EPR measurements [23].

In conclusion it is shown that the effect of high concentration of anti-site defects, which drives the transition from the kesterite-($I\bar{4}$) to the disordered kesterite-($I\bar{4}2m$) in CZTS, can be detected experimentally by changes of the position and the width of the most intensive Raman A-symmetry line: the peak at $338\,\mathrm{cm}^{-1}$ changes to a broader band at $332\,\mathrm{cm}^{-1}$. Such transformation can be induced by intense optical excitation of the electronic sub-system.

1. H. Katagiri, Thin Solid Films **480–481**, 426 (2005).

2. S. Siebentritt and S. Schorr, Prog. Photovoltaics Res. Appl. **20**, 512 (2012).

3. A. Walsh, S. Chen, S.-H. Wei, and X.-G. Gong, Adv. Energy Mater. **2**, 400 (2012).

4. D. A. R. Barkhouse, O. Gunawan, T. Gokmen et al., Prog. Photovoltaics Res. Appl. **20**, 6 (2012).

5. D. Mitzi, *2012 IEEE 38th Conference (PVSC)*, Austin, TX, USA, June 3–8, Book of Abstract., 2012.

6. S. Schorr, H.-J. Hoebler, and M. Tovar, European Journal of Mineralogy **19**, 65 (2007).

7. T. Washio, H. Nozaki, T. Fukano et al., J. Appl. Phys. **110**, 074511 (2011).

8. L. Choubrac, M. Paris, A. Lafond et al., Phys. Chem. Chem. Phys. **15**(26), 10722 (2013).

9. L. Choubrac, A. Lafond, C. Guillot-Deudon et al., Inorgan. Chem. **51**, 3346 (2012).

10. S. Chen, A. Walsh, X.-G. Gong et al., Adv. Mater. **25**, 1522 (2013).

11. D. Huang and C. Persson, Thin Solid Films, http://dx.doi.org/10.1016/j.tsf.2012.10.030.

12. S. Chen, X.-G. Gong, A. Walsh et al., Appl. Phys. Lett. **94**, 041903 (2009).

13. N. B. M. Amiri and A. Postnikov, J. Appl. Phys. **112**, 033719 (2012).

14. P. A. Fernandes, P. M. P. Salome, and A. F. da Cunha, Journal of Alloys and Compounds **509**, 7600 (2011).

15. A. Khare, B. Himmetoglu, M. Johnson et al., J. Appl. Phys. **111**, 083707 (2012).

16. X. Fontane, V. Izquierdo-Rosa, E. Saucedo et al., Journal Alloys and Compounds **539**, 190 (2012).

17. M. Ya. Valakh, O. F. Kolomys, S. S. Ponomaryov et al., Phys. Stat. Sol. RRL. **7**, 258 (2013).

18. M. Grossberg, J. Krustok, J. Raudoja, and T. Raadik, Appl. Phys. Lett. **101**, 102102 (2012).

19. T. D. Dzhafarov, Phys. Stat. Sol. a **79**, 11 (1983).

20. J. Dabrowski and M. Schefler, Phys. Rev. B **40**, 10391 (1989).

21. A. M. Brodin, S. A. Boiko, M. Ya. Valakh et al., Phys. Stat. Sol. b **150**, 557 (1988).

22. A. F. Holleman and N. Wiberg, *Inorganic Chemistry*, San Diego, Academic Press, 2001.

23. G. Bernardini, D. Borrini, A. Caneschi et al., Phys. Chem. Miner. **27**, 453 (2000).